

Physical source realization of complex source pulsed beams

Ehud Heyman^{a)} and Vitality Lomakin

Department of Electrical Engineering-Physical Electronics, Tel-Aviv University, Tel-Aviv 69978, Israel

Gerald Kaiser^{b)}

The Virginia Center for Signals and Waves, 1921 Kings Road, Glen Allen, Virginia 23060

(Received 24 June 1999; accepted for publication 21 December 1999)

Complex source pulsed beams (CSPB) are exact wave-packet solutions of the time-dependent wave equation that are modeled mathematically in terms of radiation from a pulsed point source located at a complex space-time coordinate. In the present paper, the physical source realization of the CSPB is explored. This is done in the framework of the acoustic field, as a concrete physical example, but a similar analysis can be applied for electromagnetic CSPB. The physical realization of the CSPB is addressed by deriving exact expressions for the acoustic source distribution in the real coordinate space that generates the CSPB, and by exploring the power and energy flux near these sources. The exact source distribution is of finite support. Special emphasis is placed on deriving simplified source functions and parametrization for the special case where the CSPB are well collimated. © 2000 Acoustical Society of America. [S0001-4966(00)00804-3]

PACS numbers: 43.20.Px, 43.20.Bi, 41.20.Jb, 03.50.-z [ANN]

INTRODUCTION

Complex source pulsed beams (CSPB) [also termed pulsed beams (PB) or isodiffracting PB] are exact wave-packet solutions of the time-dependent wave equation that can be modeled mathematically in terms of radiation from a pulsed point source located at a complex space-time coordinate.¹⁻³ Their properties, namely their direction, collimation, and space-time width, are determined by the complex source coordinates. Physically, however, these solutions are generated by physical source distributions (derived in this paper); hence, the complex source model may be considered as a mathematical trick to obtain compact field solutions due to these source distributions. This complex source approach has been originally introduced in the context of time-harmonic fields.⁴⁻⁷ Another approach to derive the CSPB has been derived independently in Ref. 8.

The CSPB have many properties that make them favorable wave objects within a general wave-based approach for forward and inverse problems:

- (1) They are convenient wavelets for high-resolution probing of the propagation environment, and may be used to selectively excite local scattering and diffraction phenomena (see items 2 and 4 below).
- (2) They provide benchmark solutions for scattering of collimated wave packets by canonical configurations,⁹⁻¹¹ for propagation in inhomogeneous media,^{12,13} in dispersive media,¹⁴⁻¹⁶ and in random media,^{17,18} or can be used to model practical systems involving collimated short-pulse fields.¹⁹⁻²²
- (3) They furnish a complete basis for local observable-based spectral synthesis of general transient fields, providing *a priori* localization (since only those PB propagators that pass near the space-time observation point need to be

accounted for). Several expansion schemes which apply to different source configurations have been derived in Refs. 23-28.

- (4) Finally, in view of these properties the CSPB are well-suited to wave-based data processing and local inverse scattering.^{29,30}

The *space-time localization* described above provides a systematic wave-based approach for dealing with global complexity. Concentrating on localized solutions permits the use of specific well-defined “simpler” problems from which global solutions are assembled. The CSPBs not only provide simple local wave solutions, but may also be directed in space-time to interrogate a particular subenvironment or wave phenomenon in the global conglomerate.

Other classes of wave-packet solutions *in free space* have been introduced in various disciplines. The basic ones are: solutions based on Brittingham’s “focus wave modes,”³¹⁻³⁴ “nondiffracting beams” or “X-waves”^{35,36} and “bullet”-type solutions.^{37,38} These solutions have not yet been utilized in a full “wave-based architecture” as described above.

As has been pointed out previously, the CSPB can be generated by a finite distribution of *physical sources*.² Our aim in the present paper is to explore this physical source realization. This is done here within the framework of the acoustic field which provides a concrete physical example, but a similar analysis can be applied for electromagnetic CSPB. The physical realization of the CSPB is addressed by deriving expressions for the acoustic source distributions and by exploring the power and energy flux around these sources. The finite support source functions obtained give rise to the *globally exact* CSPB. Yet, from a practical point of view, as discussed in the preceding paragraph, special emphasis is given to the parameter range where the CSPB are well collimated so that they maintain their localized wave-packet structure while propagating in the ambient en-

^{a)}Electronic mail: heyman@eng.tau.ac.il

^{b)}Electronic mail: kaiser@wavelets.com

vironment. In this special case the CSPB can be realized effectively by a truncated source distribution whose spatial support is much smaller than that of the exact CSPB. The collimated PB fields generated by the truncated aperture resemble the exact CSPB near the beam axis, but deviate from it in far off-axis region, where they are both negligible anyway.

The presentation starts with a brief summary of the relevant acoustic field equations (Sec. I) and of the basic properties of the CSPB (Sec. II). The physical realization is then explored in Sec. III from the point of view of the power and energy flow. The expressions for the source distributions are then derived in Secs. IV and V, starting with the formulation of general schemes for constructing source realizations and then applying them to calculate the CSPB sources. The presentation ends with a summary and conclusions.

I. ACOUSTIC FIELDS AND SOURCES

The linear acoustic equations for the pressure field $p(\mathbf{r}, t)$ and velocity field $\mathbf{v}(\mathbf{r}, t)$ at the space-time point $\mathbf{r} = (x, y, z) \in \mathbb{R}^3$ and time $t \in \mathbb{R}$ are

$$\frac{1}{c^2 \varrho} \partial_t p + \nabla \cdot \mathbf{v} = \sigma, \quad (1.1a)$$

$$\varrho \partial_t \mathbf{v} + \nabla p = \mathbf{f}, \quad (1.1b)$$

where $\sigma(\mathbf{r}, t)$ and $\mathbf{f}(\mathbf{r}, t)$ represent the scalar particle injection source distribution and the force distribution, respectively. Here, $c = 1/\sqrt{\kappa \varrho}$ is the wave speed in the medium, with κ and ϱ being the compressibility and density, respectively. In this paper we consider radiation in a uniform medium and, without loss of generality, we assume that $\varrho = 1$. Henceforth, we use boldface type to denote vector constituents and a \circ over a vector to denote a unit vector.

Assuming sources bounded in a volume V of finite support, the integral solution of (1.1) is

$$p = \int_V d^3 \tau' \frac{1}{4\pi R} \left[[\dot{\sigma}] + \frac{1}{c} [\dot{\mathbf{f}}] \cdot \dot{\mathbf{R}} + \frac{1}{R} [\mathbf{f}] \cdot \dot{\mathbf{R}} \right], \quad (1.2)$$

where $\mathbf{R} = \mathbf{r} - \mathbf{r}' = R \dot{\mathbf{R}}$ and $[F]$ denotes the retarded value $F(\mathbf{r}', t')|_{t' = t - R/c}$ for any function $F(\mathbf{r}', t')$. Here and henceforth, overdots and overcircles denote time derivatives and unite vectors, respectively. The solution for \mathbf{v} is readily inferred from p .

II. COMPLEX SOURCE PULSED BEAMS (CSPB)

A. The complex source coordinates

Let the source in (1.1) be

$$\mathbf{f} = 0, \quad \dot{\sigma} = 4\pi \delta(\mathbf{r} - \mathbf{r}') \psi(t - t'), \quad (2.1)$$

where $\mathbf{r}' \in \mathbb{R}^3$ and $t' \in \mathbb{R}$ define the space-time source coordinates and ψ is a given time signal. From (1.2), the solution is

$$p(\mathbf{r}, t) = \psi(t - t' - R/c)/R. \quad (2.2)$$

The CSPB is modeled analytically by extending the source coordinates (\mathbf{r}', t') in (2.1) into the complex domain. These coordinates may be expressed in general as

$$\mathbf{r}' = \mathbf{r}_0 + i\mathbf{b}, \quad |\mathbf{b}| = b, \quad (2.3a)$$

$$t' = t'_r + it'_i, \quad t'_i \geq b/c, \quad (2.3b)$$

where \mathbf{r}_0 is a *real* coordinate point that defines the center of the beam waist, \mathbf{b} is a *real* vector that defines the beam direction, and $b > 0$ is a constant which is interpreted as the collimation distance of the beam [see the discussion after (2.19)]. The condition on t'_i in (2.3b) will be explained after (2.13). Without loss of generality, we shall assume henceforth that

$$\mathbf{r}_0 = 0 \quad \text{and} \quad \mathbf{b} = \dot{\mathbf{z}}b, \quad \text{i.e.,} \quad \mathbf{r}' = (0, 0, ib), \quad (2.4a)$$

$$t' = ib/c. \quad (2.4b)$$

B. Properties of the complex distance $s(\mathbf{r})$

In order to extend (2.2) to the complex source case, we must first extend the definition of the distance R of the observer from the source. We define this distance as

$$s(\mathbf{r}) \equiv \sqrt{(x - x')^2 + (y - y')^2 + (z - z')^2}, \quad (2.5a)$$

$$= \sqrt{\rho^2 + (z - ib)^2}, \quad (2.5b)$$

$$= s_r + is_i, \quad (2.5c)$$

where (2.5a) is the general definition while (2.5b) corresponds to the special choice of the complex source coordinates in (2.4a), with $\rho = \sqrt{x^2 + y^2}$. The branch of the complex root in (2.5) is chosen with

$$\text{Re } s > 0. \quad (2.6)$$

This choice implies that $s \rightarrow r$ as $b/r \rightarrow 0$ [see (2.21)]. Other properties of s will be discussed next, where without loss of generality we consider the choice of (\mathbf{r}', t') in (2.4).

The set of branch points of s in \mathbb{R}^3 is the circle \mathcal{B} in the $z = 0$ plane, defined by $\sqrt{x^2 + y^2} = b$. In order for $s(\mathbf{r})$ to be a single-valued function of \mathbf{r} , we choose a branch cut in \mathbb{R}^3 . The choice implied by (2.6) is a flat disk (Fig. 1)

$$\mathcal{E}_0 = \{\mathbf{r}: x^2 + y^2 \leq b^2, z = 0\}, \quad (2.7)$$

although any continuous deformation of \mathcal{E}_0 leaving its boundary \mathcal{B} invariant will do the same.

The real and imaginary parts of $s = s_r + is_i$ have distinct physical roles. They can also be used as the natural coordinate system for the CSPB. For a given point $\mathbf{r} \in \mathbb{R}^3$, one finds

$$(\rho, z) = b^{-1} (\sqrt{b^2 + s_r^2} \sqrt{b^2 - s_i^2}, -s_r s_i), \quad (2.8)$$

where $s_r > 0, -b < s_i < b$.

Equation (2.8) defines an oblate spheroidal (OS) system (s_r, s_i, ϕ) with $\phi = \tan^{-1}(y/x)$ (see Fig. 1): The surfaces $s_r = \text{const}$ are spheroids \mathcal{E}_{s_r}

$$\mathcal{E}_{s_r}: \frac{x^2 + y^2}{b^2 + s_r^2} + \frac{z^2}{s_r^2} = 1, \quad s_r > 0. \quad (2.9)$$

In the limit $s_r \rightarrow 0$, \mathcal{E}_{s_r} shrinks to \mathcal{E}_0 , whereas for $s_r \gg b$ it tends to a sphere with radius $s_r = r$. Similarly, $s_i = \text{const}$ define a family of one-sided hyperboloids \mathcal{H}_{s_i}

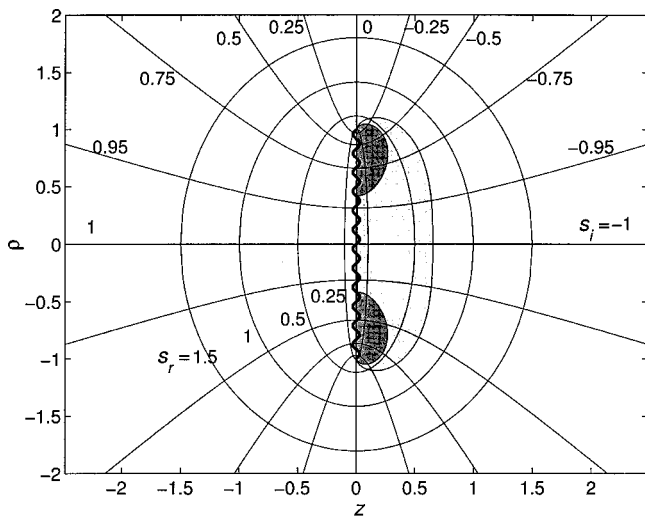


FIG. 1. The oblate spheroidal (OS) coordinate system. The shaded areas are the regions $D_{in}(\omega)$ defined in (3.16) where the energy flows inward with respect to the OS system. The light- and dark-shaded areas correspond to frequencies $kb=0.7$ and $kb=1.1$, respectively.

$$\mathcal{H}_{s_i}: \frac{x^2 + y^2}{b^2 - s_i^2} - \frac{z^2}{s_i^2} = 1, \quad -b \leq s_i \leq b. \quad (2.10)$$

These hyperboloids intersect the $z=0$ plane at \mathcal{E}_0 , and are discontinuous there with

$$s_i|_{z=\pm 0} = \mp \sqrt{b^2 - \rho^2}. \quad (2.11)$$

For $-b \leq s_i \leq 0$, \mathcal{H}_{s_i} covers the domain $z > 0$: It shrinks to the positive z axis for $s_i = -b$ and as $s_i \rightarrow 0$, it tends to the complement of \mathcal{E}_0 in the plane $z=0$. For $0 \leq s_i \leq b$, it likewise covers the domain $z < 0$.

Other properties of the OS system are mentioned in (2.16), (2.21), and in Appendix B.

C. The CSPB solution

The field due to the complex source in (2.3) is obtained as an analytic extension of the real source solution in (2.2). In order to deal with the complex propagation delays from the complex source coordinate to the real space-time observation point, one should use analytic signals that can accommodate complex time variables (see Appendix A). Henceforth, analytic signals will be denoted by the symbol $+$. The real field is then obtained by taking the real part of the analytic field solution [in fact, one may also take the imaginary part of the analytic field; see discussion after (A3)].

The analytic pressure field at a *real* space-time observation point (\mathbf{r}, t) , obtained as an analytic extension of (2.2), is given by

$$p^+(\mathbf{r}, t) = \psi^+(\tau)/s, \quad \tau = t - \gamma(\mathbf{r}), \quad (2.12)$$

with

$$\gamma = t' + s/c, \quad (2.13a)$$

$$= s_r/c + i(b + s_i)/c = \gamma_r + i\gamma_i, \quad (2.13b)$$

where (2.13b) applies for the choice of t' in (2.4b). The functions $\gamma_{r,i}(\mathbf{r})$ are the *real and imaginary time delays*.

Since $-b \leq s_i \leq b$ [see (2.10)] it follows that $\text{Im } \tau \leq 0$ for all real (\mathbf{r}, t) as required by the analyticity of ψ^+ . Recalling further that $s(\mathbf{r})$ is continuous everywhere in \mathbb{R}^3 except across the disk \mathcal{E}_0 [see the discussion in connection with (2.7)], it follows that p is an exact homogeneous solution of the time-dependent wave equation everywhere except for \mathcal{E}_0 , which is henceforth referred to as the “source disk” since it represents the location of the *real* sources that give rise to the solution in (2.12) (see Sec. V).

The solution in (2.12) has the general properties of a PB (a collimated space-time wave-packet) that emerges from \mathbf{r}_0 (here, the origin) and propagates along the beam axis \mathbf{b} (here, the positive z -axis). Confinement along the beam axis is affected by the pulse shape of ψ^+ while transverse confinement is due to the general property of analytic signals which decay in the lower half of the complex τ plane as the imaginary part of τ becomes negative. Thus, the beamwidth depends on: (a) the rate of decay of ψ^+ in the lower half of the complex τ plane (that typically depends on the pulse length), and (b) on the rate of increase of $\text{Im } \tau$ in (2.13) away from the z axis [following the discussion in (2.10), $\text{Im } \tau$ vanishes on the positive z axis and increases away from it]. The weakest signal is obtained along the negative z axis where $\text{Im } \tau = -2b/c$.

Thus, the ellipsoids \mathcal{E}_{s_r} of (2.9) are the *wavefronts* associated with the time-delay $\gamma_r = s_r/c$, while the hyperboloids \mathcal{H}_{s_i} of (2.10) are *equi-amplitude* surfaces.

1. Parametrization of the real signal

To further understand the properties of the *real* PB field, we introduce the real signal $\psi_{\gamma_i}(t)$ and its Hilbert transform $\bar{\psi}_{\gamma_i}(t)$ via [see (A3)]

$$\psi^+(t - i\gamma_i) = \psi_{\gamma_i}(t) + i\bar{\psi}_{\gamma_i}(t), \quad t \in \mathbb{R}. \quad (2.14)$$

One finds that

$$p = \text{Re } p^+ = [s_r \psi_{\gamma_i}(t - \gamma_r) + s_i \bar{\psi}_{\gamma_i}(t - \gamma_r)]/|s|^2, \quad (2.15)$$

where from (2.13b) $\gamma_r = s_r/c$ and $\gamma_i = (b + s_i)/c$. Thus, along a given hyperboloid \mathcal{H}_{s_i} [see (2.10)], the signal is gradually Hilbert transformed from $\bar{\psi}_{\gamma_i}(t - \gamma_r)/s_i$ in the near zone, where $s_r \rightarrow 0$, to $\psi_{\gamma_i}(t - \gamma_r)/s_r$ in the far zone, where $s_r \sim r \gg b$.

2. Paraxial parametrization for collimated PBs

Points near the positive beam axis, where the PB is strong, are of particular importance. From (2.5b) and (2.6) we have for $\rho \ll \sqrt{z^2 + b^2}$,

$$s \approx +[(z - ib) + \frac{1}{2}\rho^2/(z - ib)], \quad z \leq 0 \quad (2.16)$$

(note the discontinuity at \mathcal{E}_0). Substituting this into (2.12), the field near the positive z axis is given by

$$p^+(\mathbf{r}, t) = \psi^+(t - z/c - \frac{1}{2}\rho^2/c(z - ib))/(z - ib). \quad (2.17)$$

To parametrize this field, we write $1/(z-ib)=1/R(z)+i/I(z)$, where

$$R(z)=z+b^2/z, \quad I(z)=b(1+(z/b)^2), \quad (2.18)$$

thereby obtaining from (2.13)

$$\gamma_r=z/c+\rho^2/2cR(z), \quad \gamma_i=\rho^2/2cI(z). \quad (2.19)$$

Thus, $R(z)$ is identified as the radius of curvature of the PB wavefront, while $I(z)$ controls the paraxial decay away from the axis. For $z \ll b$, $I(z)$ is to leading order independent of z and the PB propagates essentially without decay or spreading, while for $z \gg b$, $\gamma_i \sim (b/2c)(\rho/z)^2$, and the wave packet diverges along the cones $\rho/z = \text{const.}$ [see (2.25)].

The *real* PB field along the z axis is given now by

$$p=[z\psi_{\gamma_i}(t-\gamma_r)-b\bar{\psi}_{\gamma_i}(t-\gamma_r)]/[z^2+b^2], \quad (2.20)$$

where $\gamma_{r,i}$ are now given in (2.19). Thus, in the near zone, the real signal is dominated by $-b^{-1}\bar{\psi}_{\gamma_i}(t-\gamma_r)$, but as z increases, it is gradually Hilbert transformed, and finally for $z \gg b$ it is dominated by $z^{-1}\psi_{\gamma_i}(t-\gamma_r)$.

3. Far-field pattern

Another important limit occurs in the far zone for $r \gg b$ where from (2.5b)

$$s=r-ib \cos \theta, \quad \cos \theta=z/r. \quad (2.21)$$

Substituting this into (2.12), we obtain

$$p(\mathbf{r},t)=r^{-1}\psi(t-r/c-i\gamma_i(\theta)), \quad \gamma_i(\theta)=(1-\cos \theta)b/c. \quad (2.22)$$

The function $\text{Re } \psi(t-\gamma_i(\theta))$ is the *time-dependent radiation pattern*. It is strongest for $\theta=0$ and decays to a minimum at $\theta=\pi$ [see the diffraction angle Θ in (2.27)].

4. Example: Analytic δ PB

The PB solutions may accommodate any analytic pulse shape. It is useful at this stage to consider an example of a particular pulse shape, namely the n -times differentiated analytic- δ pulse

$$\psi(t)=\delta^{(n)}(t-i\frac{1}{2}T)=\frac{(-)^n n!}{\pi i(t-i\frac{1}{2}T)^{n+1}}, \quad T>0. \quad (2.23)$$

It is sometimes convenient to multiply the pulses in (2.23) by $e^{i\alpha}$ with $0 \leq \alpha < \pi$ in order to change the balance between the signal and its Hilbert transform when one considers the real part of the field.

The parameter T in (2.23) is a measure of the pulse length. The spectrum of these pulses is $\hat{\psi}(\omega)=(-i\omega)^n e^{-\omega T/2}$ for $\omega>0$. The derivatives suppress the low frequencies and thus create a more localized (faster-decaying) PB in both the axial and transversal directions. In many applications, using $n \geq 2$ is required because of the higher collimation properties of the resulting PB.^{26,30} Furthermore, as will be discussed in Sec. III [see (3.16)], PB with frequency components below $\omega < c/b$ are difficult to excite.

For simplicity, however, we discuss here the PB properties for the case $n=0$ and $\alpha=0$. The real waveforms in (2.14) are given by

$$\psi_{\gamma_i}(t)=\text{Re } \delta^+(t-i(\frac{1}{2}T+\gamma_i))=\pi^{-1}\frac{\frac{1}{2}T+\gamma_i}{t^2+(\frac{1}{2}T+\gamma_i)^2}, \quad (2.24a)$$

$$\bar{\psi}_{\gamma_i}(t)=\text{Im } \delta^+(t-i(\frac{1}{2}T+\gamma_i))=-\pi^{-1}\frac{t}{t^2+(\frac{1}{2}T+\gamma_i)^2}. \quad (2.24b)$$

For a given γ_i , the half-amplitude pulse width in (2.24a) is $(T+2\gamma_i)$ and the peak amplitude (at $t=0$) is $\pi^{-1}(\frac{1}{2}T+\gamma_i)^{-1}$. Thus, the waveform is strongest and shortest for $\gamma_i=0$ (the beam axis), and decays as γ_i grows away from the axis. The half-amplitude beamwidth is therefore obtained when $\gamma_i=\frac{1}{2}T$. Substituting (2.19) for γ_i in the paraxial zone, the beam diameter is found to be

$$W(z)=W_0\sqrt{1+(z/b)^2}, \quad W_0=2\sqrt{cTb}. \quad (2.25)$$

One observes that for $0 < z < b$ the beamwidth remains essentially constant, while for $z \gg b$ it opens up along a diffraction cone whose angle $\Theta \equiv W(z)/z$ is parametrized by $\Theta=2\sqrt{cT/b}$. Collimated PB with $\Theta \ll 1$ are obtained when

$$cT/b \ll 1. \quad (2.26)$$

Note also that, under this *collimation condition*, the effective width of the source distribution, which is roughly given by W_0 [see (2.25)], is much narrower than the ‘‘exact’’ source disk \mathcal{E}_0 whose radius is b . One obtains the following rule of thumb for the relation between the pulse length T , the beamwidth at the waist W_0 , the diffraction angle Θ , and the collimation distance b

$$(W_0/b)^2=\Theta^2=4cT/b \ll 1. \quad (2.27)$$

Thus, the field properties are controlled by the PB parameter cT/b . Similar properties are obtained for other pulse types, such as nonmodulated or modulated Gaussian pulses or modulated δ pulses.

Figure 2 depicts cross sectional snapshots in the (z,ρ) plane of the axially symmetric p field of (2.12). The pulse used is a differentiated analytic delta pulse $\psi(t)=-e^{i\alpha}\delta^{(1)}(t-i\frac{1}{2}T)$ of type (2.23) and a PB parameter $cT/b=10^{-3}$ that yields a collimated PB [see (2.26)]. (Recall that it is advantageous to deemphasize the low frequencies further by using $\delta^{(2)}$ and a smaller parameter cT/b .) As mentioned in (2.23), the term $e^{i\alpha}$ is used to change the balance between the signal and its Hilbert transform. Here, α has been chosen to be $\pi/3$, which provides the ‘‘nicest’’ result (this value also provides the clearest results of the power flux analysis in Fig. 3).

The field in Fig. 2 is plotted at times $ct/b=0.2, 1$, and 2 , where the PB is localized, respectively, in the near zone $z=0.2b$, at the collimation distance $z=b$, and in the ‘‘far’’ zone $z=2b$. Note the Hilbert transform exhibited by the waveforms in the transition from the near to the far zones [recall (2.15) and (2.20)]. To demonstrate the effect of the collimation parameter cT/b , we also show in Fig. 2(d) the

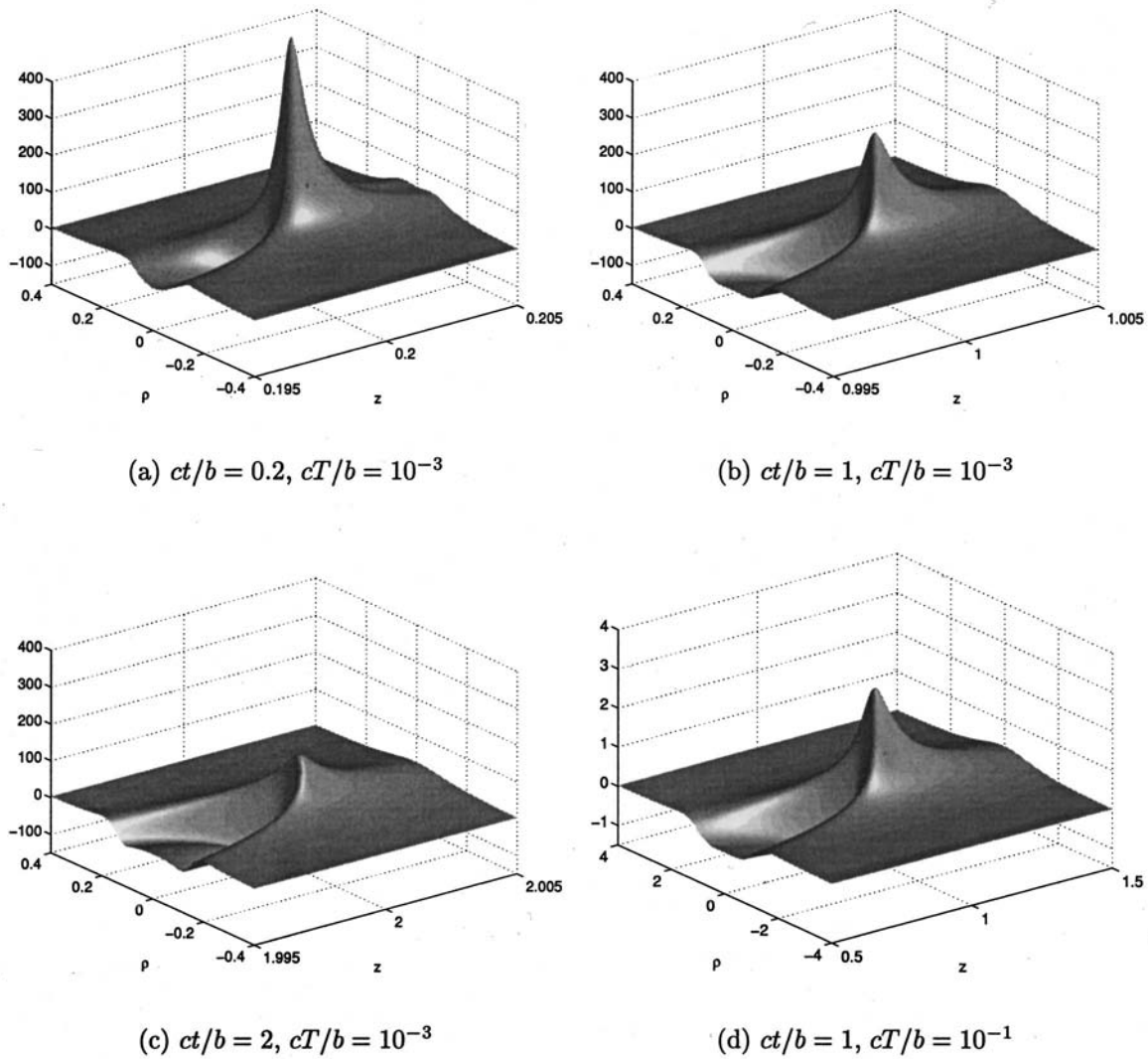


FIG. 2. Snapshots of the p field of (2.12) for a pulse $\psi(t) = -e^{i\alpha} \delta^{(1)}(t - i\frac{1}{2}T)$ with $\alpha = \pi/3$. The plots show cross-sectional cuts of the axially symmetric field in the (z, ρ) plane where all axes are normalized with respect to b . PB parameter: $cT/b = 10^{-3}$ in subfigures (a)–(c) (collimated PB), and $cT/b = 10^{-1}$ in (d) (noncollimated PB). Observation times: (a) $ct/b = 0.2$ (near zone); (b) $ct/b = 1$ (intermediate zone); (c) $ct/b = 2$ (far zone); (d) $ct/b = 1$.

CSPB field for the parameter $cT/b = 10^{-1}$. In this case the solution in (2.12) is still exact but the parametrization in (2.25)–(2.27) is not valid (note the different space–time and field–amplitude scales used in this case).

III. THE POWER AND ENERGY FLUX

A. The \mathbf{v} field

The \mathbf{v} field is needed in the calculation of the power flux [see (3.7)]. Outside the source domain, \mathbf{v} is calculated from p of (2.12) via $\mathbf{v} = -\partial_t^{(-1)} \nabla p$, giving

$$\mathbf{v}(\mathbf{r}, t) = \nabla_s \{ \psi(\tau)/cs + \psi^{(-1)}(\tau)/s^2 \}, \quad (3.1)$$

$$\nabla_s = (\mathbf{r} - i\mathbf{b})/s, \quad (3.2)$$

where $\psi^{(-1)}(t) = \int_{-\infty}^t dt' \psi(t')$ and τ is defined in (2.13). The real (physical) expression for \mathbf{v} is [cf. (2.15)]

$$\begin{aligned} \mathbf{v} = \nabla_{s_r} \{ & p/c + [(r^2 - b^2)\psi_{\gamma_i}^{(-1)} - 2zb\bar{\psi}_{\gamma_i}^{(-1)}]/|s|^4 \} \\ & - \nabla_{s_i} \{ \bar{p}/c + [2zb\psi_{\gamma_i}^{(-1)} + (r^2 - b^2)\bar{\psi}_{\gamma_i}^{(-1)}]/|s|^4 \}, \end{aligned} \quad (3.3)$$

where $p = (s_r \psi_{\gamma_i} + s_i \bar{\psi}_{\gamma_i})/c|s|^2$ is the real p field [see (2.15)], the overbars denote Hilbert transforms of the respective waveforms [see (2.14)], and ψ_{γ_i} stands for $\psi_{\gamma_i}(t - \gamma_r)$, etc. Note in (3.3) that ∇_{s_r} represents *outward* power flow lines *normal* to the wavefronts \mathcal{E}_{s_r} , while ∇_{s_i} represents *transverse* flow lines along the wavefronts, leading from the positive z axis to the negative z axis. In deriving (3.3) we used the relations in (B1). Expressions for $\nabla_{s_{r,i}}$ are given in (B2)–(B4).

In order to estimate the role of the various terms in (3.1) and (3.3) we assume that ψ is a short pulse with pulse length T , so that near the positive z axis where $\gamma_i \approx 0$ we have $\psi^{(-1)}(\tau)/\psi(\tau) \sim O(T)$. Recalling from (2.16) that near the axis $s \approx z - ib$, we find that the ratio between the second and first terms inside the braces in (3.1) is

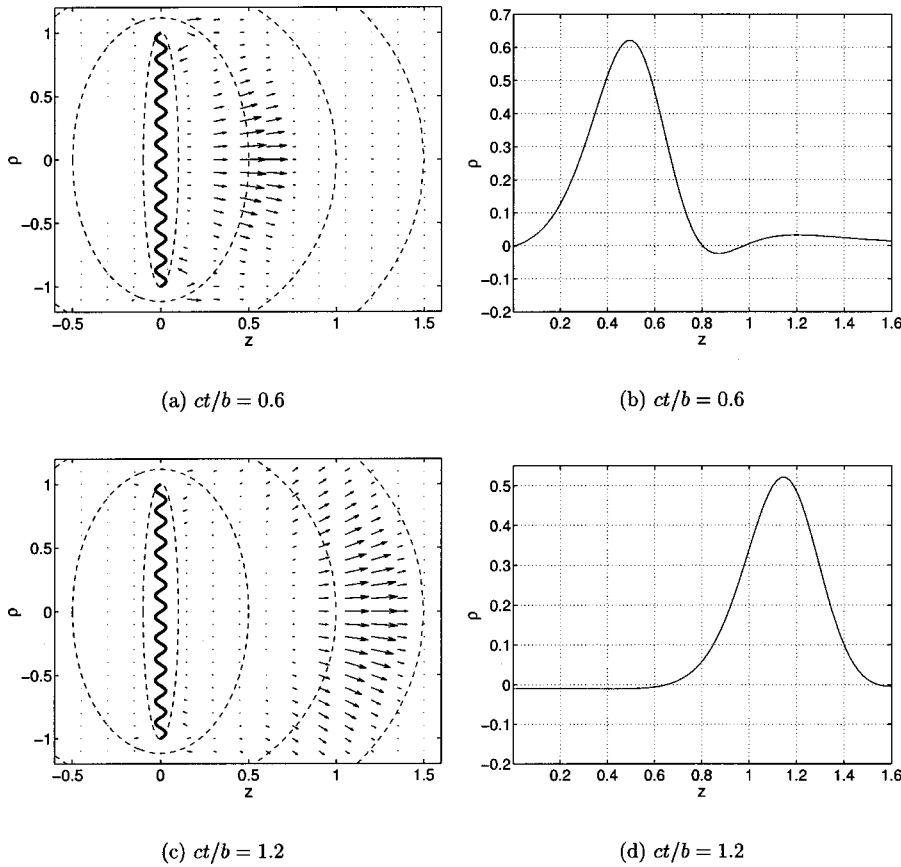


FIG. 3. Snapshots of the power flow \mathbf{P} at times $ct/b=0.6$ and 1.2 . Here, $\psi^+(t) = e^{i\alpha} \delta^{(1)}(t - i\frac{1}{2}T)$ as in Fig. 2, but with $cT/b=1.2$ (highly noncollimated PB) and $\alpha = \pi/3$. (a) and (c): Distributions of \mathbf{P} in the (z, ρ) plane (all axes are normalized with respect to b). For clearer interpretation, the results are superimposed on the ellipsoidal wavefront corresponding to the coordinate system of Fig. 1. The arrows describe the size and direction of \mathbf{P} . (b) and (d): snapshot of P_z on the z axis at the same times.

$$[\psi^{(-1)}(\tau)/s^2]/[\psi(\tau)/cs] \sim O[cT/|z-ib|]. \quad (3.4)$$

In the far zone, the ratio on the right-hand side of (3.4) is much smaller than unity. Under the collimation condition $cT \ll b$ in (2.26), this term is much smaller than unity also in the near zone (i.e., along the entire z axis). Under these conditions, the terms containing $\psi^{(-1)}$ in (3.1) may be neglected for all $z > 0$ so that (3.3) becomes

$$\mathbf{v} \approx (\nabla s_r) p/c - (\nabla s_i) \bar{p}/c, \quad (3.5)$$

where p is given by (2.20) for points near the z axis. Note from (2.16) with (2.18) that near the z axis $\nabla s_r \approx \dot{\mathbf{z}} + \boldsymbol{\rho}/R(z) \rightarrow \dot{\mathbf{z}}$ and $\nabla s_i \approx \boldsymbol{\rho}/I(z) \rightarrow \mathbf{0}$, where $\boldsymbol{\rho} = (x, y)$. Recall also that ∇s_r is orthogonal to the wavefronts whose local radius of curvature is $R(z)$.

In the far zone, we note from (2.21) that $\nabla s \approx \nabla s_r \rightarrow \dot{\mathbf{r}}$, hence

$$\mathbf{v} \approx \dot{\mathbf{r}} p/c, \quad (3.6)$$

where here p is given in (2.22).

B. The power and energy flux

The power flux is defined as

$$\mathbf{P}(\mathbf{r}, t) = p(\mathbf{r}, t) \mathbf{v}(\mathbf{r}, t). \quad (3.7)$$

The expression obtained by inserting (2.15) and (3.3) is quite complicated. It is therefore convenient to explore the energy flux

$$\mathbf{E}(\mathbf{r}) = \int_{-\infty}^{\infty} dt \mathbf{P}(\mathbf{r}, t). \quad (3.8)$$

One finds that

$$\mathbf{E}(\mathbf{r}) = \nabla s_r \|\psi_{\gamma_i}\|^2/c|s|^2 + \langle \psi_{\gamma_i}, \bar{\psi}_{\gamma_i}^{(-1)} \rangle (s_i \nabla s_r - s_r \nabla s_i)/|s|^4, \quad (3.9)$$

where $\langle f, g \rangle = \int_{-\infty}^{\infty} dt f(t)g(t)$ for any two real functions f and g . In deriving (3.9) we used the following relations which apply for any real f and its Hilbert transform \bar{f} : $\langle f, f \rangle = \langle \bar{f}, \bar{f} \rangle = \|f\|^2$, $\langle f, \bar{f} \rangle = \langle \bar{f}, f \rangle = 0$, and $\langle f, \dot{f} \rangle = 0$ (since f vanishes at $t = \pm\infty$).

In the far zone, the second term in (3.9) vanishes and the outward radiative energy is described only by the first term. Both terms are large in the near zone, in particular near \mathcal{B} where s vanishes, and the field there dominated by strong reactive fields. The concept of *time-dependent reactive field and energy* has been introduced and analyzed in Ref. 39 in the context of electromagnetic fields. Using time-dependent spherical wave (multipole) expansion, it has been shown that the time-dependent power radiated by an antenna consists of radiative and reactive pulses. The radiative power is a *positive outgoing pulse* and is unchanged as it propagates away from the source (carries the same energy). The reactive power pulse, on the other hand, is strong in the near zone and vanishes in the far zone. It carries no net energy: at early times it propagates out and builds up a transient energy near the source, but after the radiative pulse has passed it discharges the energy back to the source region.

This phenomenology is demonstrated in Fig. 3, which depicts snapshots of \mathbf{P} . In order to be able to discern the off-axis properties of \mathbf{P} and the low-frequency phenomena discussed in (3.16) below, the PB parameters have been cho-

sen to yield a highly noncollimated field. Specifically, $\psi(t)$ is the differentiated analytic δ used in Fig. 2, but with the PB parameter $cT/b=1$. Figure 3(a) and (c) show the distribution of \mathbf{P} in the (z, ρ) plane at times $ct/b=0.6$ and 1, while 3(b) and (d) show plots of P_z along the z axis at the same observation times. Note from Fig. 3(a) and (c) that the flow lines in the near zone deviate from the normal to the wavefronts \mathcal{E}_{s_r} [see, e.g., (3.9)], and in particular the relatively strong “inward” flow near \mathcal{B} . As discussed in (3.16) below, this inward flow is strong near \mathcal{B} , but the low-frequency components propagate inward also in front of the entire source disk \mathcal{E}_0 (see the shaded zones in Fig. 1). Indeed, in view of the relatively low-frequency content of the signal ψ chosen, the inward flow of reactive energy is readily observed as the negative part of P_z behind the leading part of the signal in Fig. 3(d).

C. Frequency-domain analysis of the energy flow

We shall explore the constituents discussed above in the frequency domain (FD). The FD expressions corresponding to the field solutions in (2.12) and (3.1) are

$$\hat{p}(\mathbf{r}, \omega) = \hat{\psi}(\omega) s^{-1} e^{iks + i\omega t'} = \hat{\psi}(\omega) s^{-1} e^{i\omega(\gamma_r + i\gamma_i)}, \quad (3.10a)$$

$$\hat{\mathbf{v}}(\mathbf{r}, \omega) = \nabla s [c^{-1} - (i\omega s)^{-1}] \hat{p}(\mathbf{r}, \omega), \quad (3.10b)$$

where $k = \omega/c$ and the carets denote field constituents with a suppressed time dependence $e^{-i\omega t}$ with $\omega > 0$ (for $\omega < 0$, one should take the complex conjugate of these expressions). Here $\hat{\psi}(\omega)$ is the (rather arbitrary) spectrum of the pulse $\psi(t)$. In the high-frequency regime such that $kb \gg 1$, the solution in (3.10) has the characteristics of a time-harmonic Gaussian beam (see, e.g., Refs. 4–7 and 2) but we shall not dwell here on this interpretation.

Using (3.10) in conjunction with (3.7) and (3.8), we obtain

$$\begin{aligned} \mathbf{E}(\mathbf{r}) &= \frac{1}{\pi} \operatorname{Re} \int_0^\infty d\omega \hat{p}(\mathbf{r}, \omega) \hat{\mathbf{v}}^*(\mathbf{r}, \omega) \\ &= \frac{1}{\pi} \operatorname{Re} \int_0^\infty d\omega |\hat{\psi}|^2 |s|^{-2} e^{-2\omega\gamma_i} (c^{-1} + (i\omega s^*)^{-1}) \nabla s^*, \end{aligned} \quad (3.11)$$

where the asterisks denote a complex conjugate.

Next, we consider the total energy radiated out of the spheroidal wavefront \mathcal{E}_{s_r} ,

$$E_{\text{rad}}(s_r) = \oint_{\mathcal{E}_{s_r}} \mathbf{E} \cdot d\mathbf{S}, \quad (3.12)$$

where $d\mathbf{S}$ is an area element on \mathcal{E}_{s_r} . Substituting (3.11), we note that on \mathcal{E}_{s_i} we have $\nabla s \cdot d\mathbf{S} = |\nabla s_r| dS$, where $|\nabla s_r|$ is given in (B2) and $dS = h_{s_i} h_\phi ds_i d\phi$, where the metric coefficients are given in (B5). The ϕ -integration yields 2π . Recalling that s_i changes from $-b$ on the positive z axis to b on the negative axis, we end up with

$$E_{\text{rad}}(s_r) = \int_0^\infty d\omega \int_{-b}^b ds_i E_{s_r}(s_r, s_i, \omega) \quad (3.13a)$$

with

$$E_{s_r}(s_r, s_i, \omega) = \frac{2}{bc} |\hat{\psi}|^2 e^{-2k(b+s_i)} \frac{b^2 + s_r^2}{s_r^2 + s_i^2} \left[1 + \frac{s_i/k}{s_r^2 + s_i^2} \right]. \quad (3.13b)$$

E_{s_r} is the spectral density of the “outward” (i.e., the s_r) component of \mathbf{E} .

The s_i integral in (3.13) may readily be evaluated by rewriting (3.13b) in the form

$$E_{s_r}(s_r, s_i, \omega) = \frac{-1}{\omega b} |\hat{\psi}|^2 (b^2 + s_r^2) \frac{\partial}{\partial s_i} \left[\frac{e^{-2k(b+s_i)}}{s_r^2 + s_i^2} \right], \quad (3.14)$$

which provides a closed-form result for the outward flow between any two hyperbolas \mathcal{H}_{s_i} . Integrating over the full domain (i.e., from $s_i = -b$ to b), we end up with

$$E_{\text{rad}} = \int_0^\infty d\omega |\hat{\psi}|^2 \frac{1 - e^{-4kb}}{\omega b}, \quad (3.15)$$

i.e., $E_{\text{rad}} > 0$ and is independent of s_r as expected. Note that under the collimation condition in (2.26), most of the signal energy is concentrated in the high-frequency range $kb \gg 1$ where the exponent in (3.15) is negligible.

While the *total* energy E_{rad} flows outward, the *local* energy flux E_{s_r} may, in some regions, flow inward. From (3.13b) the region $\mathcal{D}_{\text{in}}(\omega)$ of inward energy flow is described by

$$\mathcal{D}_{\text{in}}(\omega): \frac{s_i/k}{s_r^2 + s_i^2} < -1. \quad (3.16)$$

In general, $\mathcal{D}_{\text{in}}(\omega)$ is located in front of \mathcal{E}_0 (where $s_i < 0$). A detailed analysis of (3.16) reveals that for frequencies such that $kb > 1$, $\mathcal{D}_{\text{in}}(\omega)$ has the shape of a ring in front of \mathcal{E}_0 whose boundary on \mathcal{E}_0 is given by $-k^{-1} < s_i < 0$ (see the dark-shaded region in Fig. 1). In particular, in the high-collimation range where $kb \gg 1$, this ring becomes concentrated near \mathcal{B} . For low frequencies such that $kb < 1$, on the other hand, $\mathcal{D}_{\text{in}}(\omega)$ covers the entire front face of \mathcal{E}_0 (see the light-shaded region in Fig. 1). Recall though that at any given frequency, the *total* energy flows outward through \mathcal{E}_{s_r} , as implied by (3.15). It follows that at low frequencies, the energy is emitted by the back face of \mathcal{E}_0 : part of it flows around \mathcal{E}_0 and is absorbed by the front face, while the other radiates outward through \mathcal{E}_{s_r} .

The analysis above implies that for practical synthesis of the CSPB, the frequency spectrum of ψ should be concentrated at frequencies such that $kb \gg 1$. Recalling that the effective width of the aperture in this range is $W_0(\omega) = \sqrt{b/k}$ [cf. (2.25) and Ref. 2], it follows that for $kb > 2$, W_0 is narrower than the inner radius of $\mathcal{D}_{\text{in}}(\omega)$ which is given by $s_i = -k^{-1}$ [see (3.16)]. Under these conditions the aperture can be truncated about the effective aperture W_0 of (2.25), giving essentially the same field as the *exact* CSPB which is generated by the entire source disk \mathcal{E}_0 .

IV. SURFACE SOURCES AND EQUIVALENT SOURCES

We start by recalling the field discontinuity conditions implied by (1.1). Let \mathcal{S} be a given surface carrying surface sources (σ_s, f_s) , i.e.,

$$\sigma = \sigma_s(\mathbf{r}_s, t) \delta(n), \quad \mathbf{f} = \dot{\mathbf{n}} f_s(\mathbf{r}, t) \delta(n), \quad (4.1)$$

where $\mathbf{r}_s \in \mathcal{S}$, $\dot{\mathbf{n}}$ is the normal to \mathcal{S} at \mathbf{r}_s , pointing from side 1 to side 2 of \mathcal{S} , and n is the coordinate along $\dot{\mathbf{n}}$. The field discontinuities implied by these sources are found from (1.1) to be

$$\dot{\mathbf{n}} \cdot (\mathbf{v}_2 - \mathbf{v}_1) = \sigma_s, \quad p_2 - p_1 = \dot{\mathbf{n}} \cdot \mathbf{f}_s \equiv f_s, \quad (4.2)$$

where (\mathbf{v}_i, p_i) are the limiting value of (\mathbf{v}, p) at side i of \mathcal{S} .

Next, let \mathcal{S} be a closed surface that encloses all the sources to the field. We would like to synthesize the field outside \mathcal{S} due to the sources inside \mathcal{S} in terms of surface sources on it. As will be shown, there exist various realizations of these sources; of particular interest are those involving only σ or \mathbf{f} sources. These alternative realizations are obtained by choosing inside \mathcal{S} an *arbitrary solution* of the homogeneous field equation, denoted as $(p^{\text{in}}, \mathbf{v}^{\text{in}})$. Using (4.2), the surface sources are now given by

$$\sigma_s = \dot{\mathbf{n}} \cdot (\mathbf{v} - \mathbf{v}^{\text{in}})|_S, \quad f_s = (p - p^{\text{in}})|_S, \quad (4.3)$$

where $\dot{\mathbf{n}}$ is an outward normal to \mathcal{S} . Substituting (4.3) into (1.2), we obtain

$$p = \int_S dS' \frac{1}{4\pi R} [[\dot{\sigma}_s] + (c^{-1}[\dot{f}_s] + R^{-1}[f_s]) \dot{\mathbf{n}}' \cdot \dot{\mathbf{R}}]. \quad (4.4)$$

This integral synthesizes the true field (p, \mathbf{v}) at points outside \mathcal{S} and the arbitrarily chosen field $(p^{\text{in}}, \mathbf{v}^{\text{in}})$ at points inside \mathcal{S} .

A. Kirchhoff realization

As mentioned before, different source realizations are generated by choosing different homogeneous solutions $(p^{\text{in}}, \mathbf{v}^{\text{in}})$ in (4.3). One such choice,

$$p^{\text{in}} = 0, \quad \mathbf{v}^{\text{in}} = \mathbf{0}, \quad (4.5)$$

gives rise to what will be identified below as the Kirchhoff realization. Using (4.5) and (4.3), the Kirchhoff sources are

$$\sigma_s = \dot{\mathbf{n}} \cdot \mathbf{v}|_S = -\partial_n \partial_t^{-1} p|_S, \quad f_s = p|_S, \quad (4.6)$$

where in the second expression for σ_s we used (1.1b) to replace the limiting value of \mathbf{v} outside \mathcal{S} by the value of p there. When the sources in (4.6) are substituted into (4.4), we obtain the true field outside \mathcal{S} and a null contribution inside \mathcal{S} .

Using (4.6) in (4.4), one obtains the conventional Kirchhoff integral representation for the radiating field in terms of the values of p and $\partial_n p$ on \mathcal{S} , which is usually obtained by using the scalar wave equation for p in conjunction with Green's theorem.⁴⁰ Thus, Eq. (4.6) provides the surface source realization of this formula.

B. Integral equations for alternative source realizations

Equation (4.4) synthesizes the field outside \mathcal{S} due to the sources inside \mathcal{S} in terms of both σ_s and f_s sources. Alternative formulations are obtained if one chooses different values for $(p^{\text{in}}, \mathbf{v}^{\text{in}})$. We shall look, in particular, for realizations such that either f_s or σ_s in (4.3) vanishes identically on \mathcal{S} . These sources are determined via an integral equation as described below.

We start by expressing the field (4.4) for the special case of the sources in (4.6) as a sum of two terms: $p = p^\sigma + p^f$ denoting, respectively, the fields due to the f_s and σ_s sources in (4.6). Substituting (4.6) in (4.4), these fields may be expressed in terms of the known field p outside \mathcal{S}

$$p^f = \int_S dS' \frac{1}{4\pi R} (c^{-1}[\dot{p}] + R^{-1}[p]) \dot{\mathbf{n}}' \cdot \dot{\mathbf{R}}, \quad (4.7)$$

$$p^\sigma = \int_S dS' \frac{-1}{4\pi R} [\partial_n p].$$

The σ_s -only realization involves the σ_s sources in (4.6) plus an additional term denoted as σ_s^f that gives rise to the *known* field p^f outside \mathcal{S} . σ_s^f is therefore calculated via the integral equation on \mathcal{S}

$$\int_S dS' \frac{1}{4\pi R} [\dot{\sigma}_s^f] = p^f(\mathbf{r}, t), \quad \mathbf{r}, \mathbf{r}' \in \mathcal{S}, \quad (4.8)$$

where p^f is given in (4.7) in terms of the known field p on the outer side of \mathcal{S} . Note that the kernel on the left-hand side of (4.8) is singular at $\mathbf{r}' = \mathbf{r}$, but this singularity can be extracted explicitly using principal value integration.

The solution of (4.8) is not unique. Recalling from (4.3) that the internal field $(p^{\text{in}}, \mathbf{v}^{\text{in}})$ in the σ_s -only realization satisfies $p^{\text{in}}|_S = p|_S$ where p is the known pressure field outside \mathcal{S} , it follows that the null space of (4.8) is described by internal field solutions that satisfy $p^{\text{in}}|_S = 0$. Such solutions are possible at discrete frequencies ω_n , $n = 1, 2, \dots$, which are the *internal resonance frequencies* of \mathcal{S} for the ‘‘soft’’ boundary condition $p^{\text{in}}|_S = 0$. The solution of (4.8) can therefore be augmented by a discrete set of eigensolutions of the form $\sigma_s^f(\mathbf{r}, t) = \sum_n \text{Re } a_n \sigma_{s_n}(\mathbf{r}) e^{-i\omega_n t}$, which do not affect the field outside \mathcal{S} . A unique solution is obtained by imposing another criterion, say a minimum energy condition. We shall not consider this subject here.

Similarly, the f_s -only realization involves the f_s sources of (4.6) plus an additional term f_s^σ that generates the p^σ field outside \mathcal{S} . f_s^σ is found via the integral equation on \mathcal{S}

$$\int_S dS' \frac{1}{4\pi R} (c^{-1}[\dot{f}_s^\sigma] + R^{-1}[f_s^\sigma]) \dot{\mathbf{n}}' \cdot \dot{\mathbf{R}} = p^\sigma(\mathbf{r}, t), \quad \mathbf{r}, \mathbf{r}' \in \mathcal{S}, \quad (4.9)$$

where p^σ is given in (4.7) in terms of the known field p on the outer side of \mathcal{S} . As discussed after (4.8), the solution of (4.9) is not unique: its null space is described by the internal resonance frequencies associated the ‘‘hard’’ boundary condition $\partial_n p^{\text{in}}|_S = 0$.

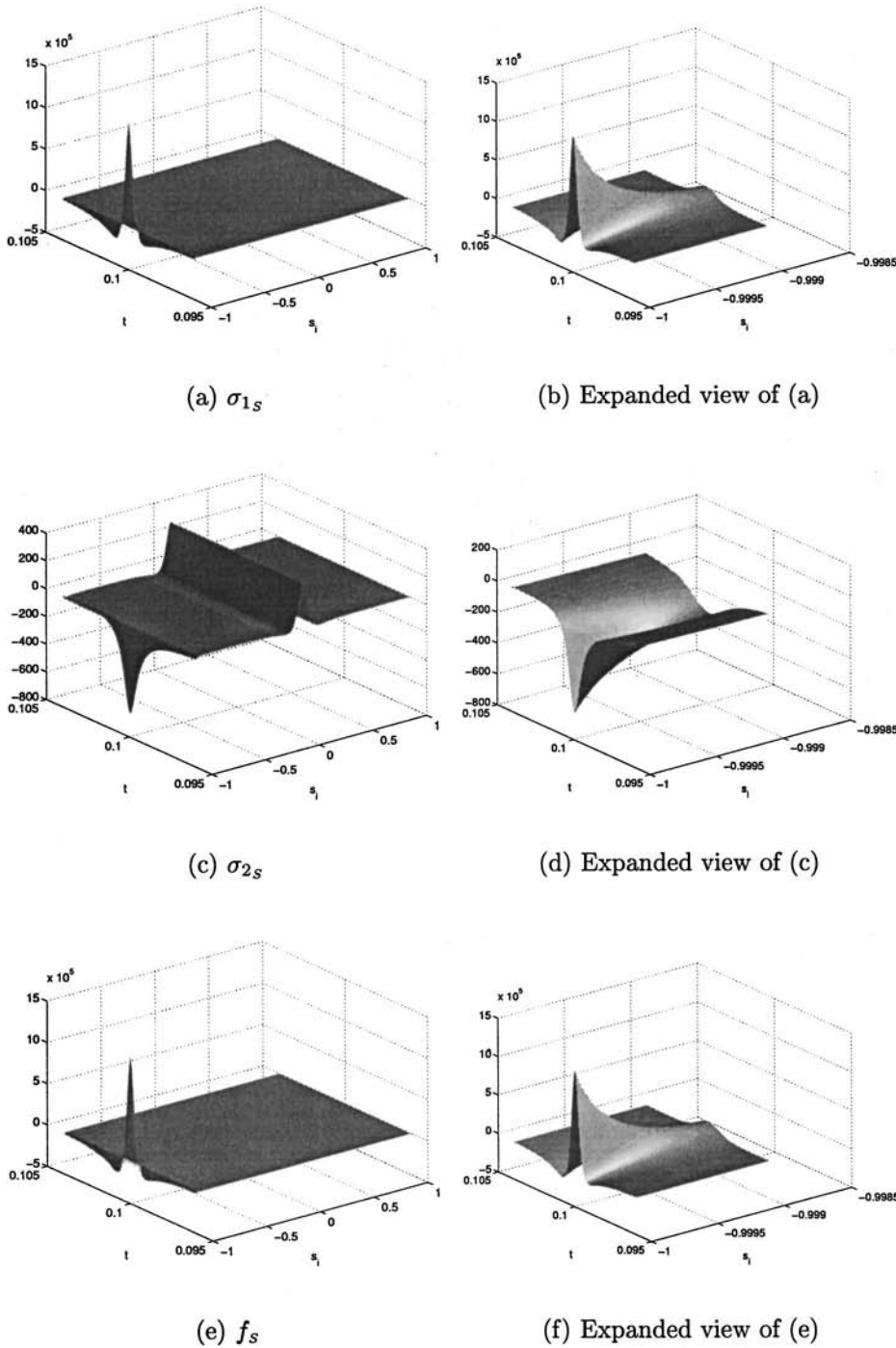


FIG. 4. Waveforms of the surface sources in (5.1) on $S=\mathcal{E}_{s_r}$ with $s_r=0.1b$. The waveforms are depicted in the (ct, s_i) plane with s_i , the coordinate along \mathcal{E}_{s_r} , varies from $-b$ on the positive z axis to b on the negative axis. (a) and (b): σ_{1s} ; (c) and (d): σ_{2s} ; (e) and (f): f_s . The pulse ψ is the differentiated analytic δ used in Fig. 2 with high-collimation parameter $ct/b=10^{-3}$.

V. SOURCE DISTRIBUTIONS FOR THE CSPB

It is convenient to consider a source realization on the ellipsoid \mathcal{E}_{s_r} of (2.9) for a given $s_r > 0$. Substituting (2.12) and (3.1) into (4.6), we obtain

$$\sigma_s = |\nabla_{s_r}| \text{Re}\{\psi^+(\tau)/cs + \psi^{(-)}(\tau)/s^2\}, \quad (5.1a)$$

$$f_s = \text{Re}\{\psi^+(\tau)/s\}, \quad (5.1b)$$

where s , τ , and $|\nabla_{s_r}|$ are given in (2.5b), (2.12), and (B2), respectively. These expressions are functions of s_i , which serves as a coordinate along \mathcal{E}_{s_r} .

Explicit expressions are obtained for the special case when \mathcal{E}_{s_r} shrinks to the source disk \mathcal{E}_0 of (2.7). Denoting values on the front and back faces of \mathcal{E}_0 by the superscript \pm , respectively, we find that

$$s^\pm = \mp i\eta, \quad \gamma^\pm = i(b \mp \eta)/c, \quad \text{where } \eta = \sqrt{b^2 - \rho^2}. \quad (5.2)$$

Substituting (2.12) and (3.1) into (4.6), we obtain

$$\sigma_s^\pm = \frac{b}{\eta} \text{Re}\{\pm i\psi^+[t - i(b \mp \eta)]/\eta c - \psi^{(-)}[t - i(b \mp \eta)]/\eta^2\}, \quad (5.3a)$$

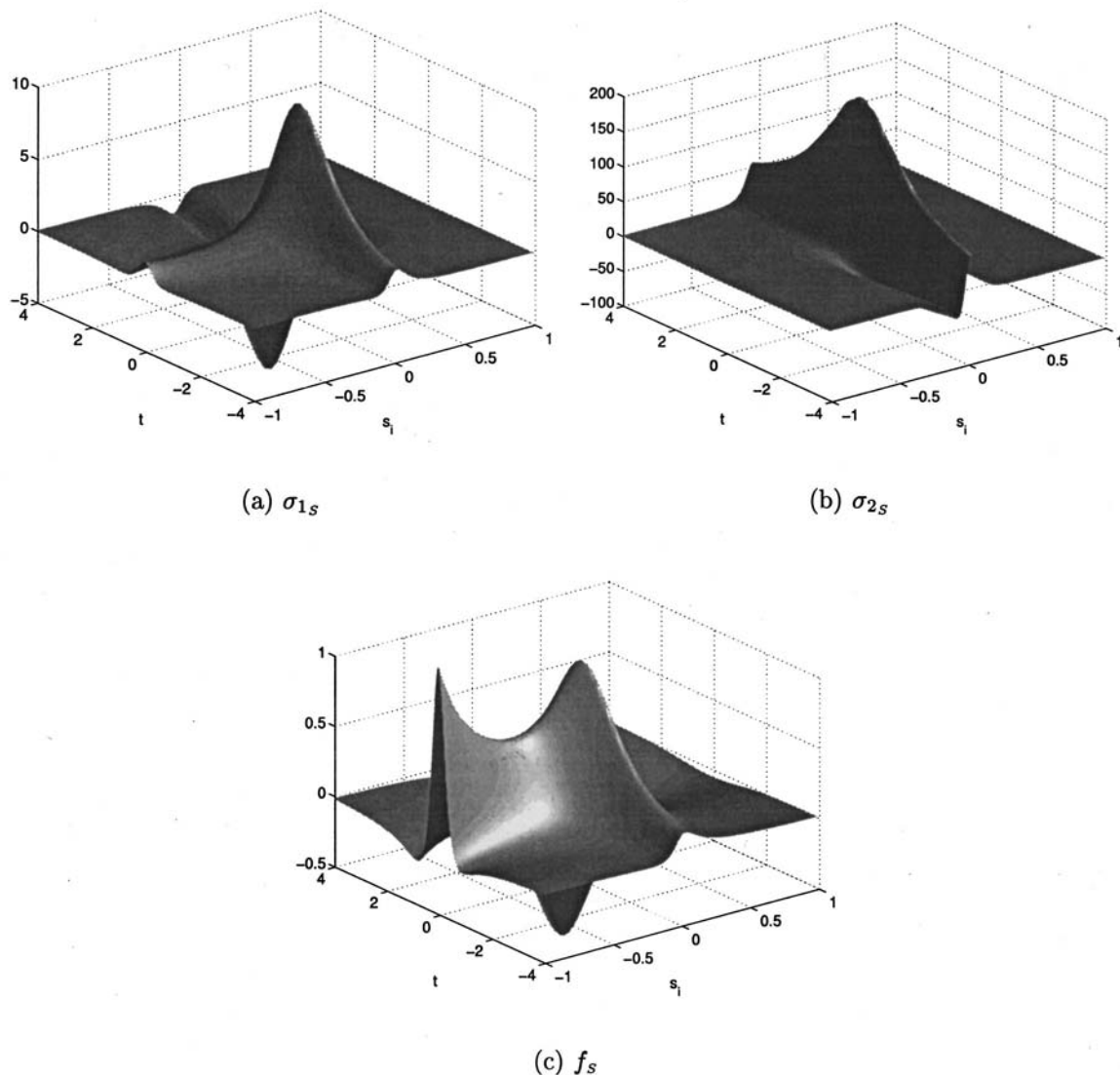


FIG. 5. Same as Fig. 4, but for noncollimated source with $cT/b=1$.

$$f_{z_s}^{\pm} = \pm p | \varepsilon_0^{\pm} = \text{Re}\{i\psi[t - i(b \mp \eta)]/\eta\}, \quad (5.3b)$$

where the upper and lower signs correspond to sources on the front and back face of \mathcal{E}_0 , respectively, while $f_{z_s}^{\pm}$ in the last expression denotes the z component of the \mathbf{f}_s source on the front and back faces of \mathcal{E}_0 . Note also the algebraic singularity of the sources at $\rho=b$ on the circle \mathcal{B} .

Special attention should be given to the collimated case (2.26) which is the most important one for practical applications. We note that in this case the relevant part of the source is concentrated within the *effective aperture* W_0 (2.25) on the front face of \mathcal{E}_0 , which is much narrower than the entire disk \mathcal{E}_0 [see (2.27)]. Furthermore, under the collimation condition the contribution of the second term in σ_s is negligible [see the discussion in (3.4)]. Finally, from (5.2) it follows that for $\rho \ll b$, $\gamma_i^+ \approx \rho^2/2cb$, while $\gamma_i^- \approx 2ib/c$, hence in (5.3) $\sigma_s^+ \gg \sigma_s^-$ and $f_{z_s}^+ \gg f_{z_s}^-$. Thus, Eq. (5.3) reduces to the simplified explicit expression for effective sources

$$c\sigma_s = f_{z_s} = b^{-1} \text{Re}\{i\psi(t - i\rho^2/2cb)\}, \quad \rho \sim O(W_0). \quad (5.4)$$

These simplified sources generate a strong PB field along the positive z axis that behaves paraxially like the PB in (2.17) [or (2.20)]. In all other directions, the resulting field is weak but due to the approximation in (5.4) it does not have the exact known form of (2.12).

Alternatively, one may use *only* the σ_s or the f_s sources in (5.4). This generates collimated PB along both the positive and the negative z directions: From (4.4), the σ_s source radiates symmetrically in both directions while the f_s source radiates antisymmetrically. Taken together, the contributions of σ_s and of f_s enhance each other in the positive direction and cancel each other in the negative direction, thereby radiating a strong PB field only along the positive z axis and a weak field elsewhere.

Figures 4 and 5 depict the surface sources of the CSPB realized on an ellipsoidal wavefront $\mathcal{S} = \mathcal{E}_{s_r}$ as in (5.1). Here, s_r is taken to be $0.1b$ so that \mathcal{E}_{s_r} is close to the branch disk \mathcal{E}_0 (see Fig. 1). The waveforms are depicted in the (ct, s_i) plane with s_i being a coordinate along \mathcal{E}_{s_r} (s_i varies from $-b$ on the positive z axis to b on the negative axis). The first and

second terms in (5.1a) are termed σ_{1_s} and σ_{2_s} , respectively. The pulse ψ is the differentiated analytic δ used in Figs. 2 and 3. In Fig. 4 we use a short pulse with $cT/b = 10^{-3}$ which yields a collimated PB, while in Fig. 5 $cT/b = 1$, yielding a noncollimated field. Note that the *effective* width of the source distribution in Fig. 4 agrees with the estimates for W_0 in (2.25); hence, the sources there can be truncated and described by the simpler expressions in (5.4). In Fig. 5, on the other hand, the source distribution is much wider. In this case one also observes the relatively strong sources at points near $\mathcal{B}(s_i \approx 0)$, which are insignificantly small under the collimation condition in Fig. 4. These sources become stronger for smaller s_r , and become singular when \mathcal{S} shrinks to the branch disk \mathcal{E}_0 , yet their contribution is insignificant in the collimation condition.

VI. SUMMARY AND CONCLUSIONS

Our aim in the present paper has been to explore this physical source realization of the CSPB. This has been done within the framework of the acoustic field, by deriving expressions for the acoustic source distributions and by exploring the power and energy flux near these sources. The surface sources have been derived via the field equivalence theorems in Sec. IV. The exact source solutions derived in (5.1) [or (5.3)] generate the *globally exact* CSPB. Yet, from a practical point of view special emphasis has been given to the parameter range $cT \ll b$ [see (2.26)]; T is the pulse length and b is the collimation distance) where the CSPB is well collimated: in this special case the CSPB can be realized effectively by the simple truncated source distribution in (5.4) whose spatial support W_0 of (2.25) is much smaller than the source support of the exact CSPB.

In order to further clarify the properties of source realization, we have also explored the power flux near the sources. It has been shown [see (3.16)] that at high frequencies such that $kb \gg 1$ (k is the wave number) the energy is emitted by a narrow aperture on the front face of the source disk \mathcal{E}_0 . At low frequencies, on the other hand, the energy is emitted by the back face of \mathcal{E}_0 : part of it flows around \mathcal{E}_0 and is absorbed by the front face, while the rest radiates outward through \mathcal{E}_{s_r} . Thus, for practical synthesis the frequency spectrum of the CSPB should be concentrated in the high-frequency regime, which supports the conclusions of the preceding paragraph.

ACKNOWLEDGMENTS

This work is supported in part by the U.S. Air Force Office of Scientific Research under Grant No. F49620-98-C-0013, managed by The Virginia Center for Signals and Waves, and in part by the Israel Science Foundation under Grant No. 404/98.

APPENDIX A: ANALYTIC SIGNALS

In order to deal with the complex propagation delays implied by the complex sources, one needs to use analytic signals that can accommodate complex time variables. For a

given real signal $\psi(t)$, $t \in \mathbb{R}$, with frequency spectrum $\hat{\psi}(\omega)$, the dual analytic signal $\psi^+(\tau)$ is defined via the one-sided inverse Fourier transform

$$\psi^+(\tau) = \frac{1}{\pi} \int_0^\infty d\omega e^{-i\omega\tau} \hat{\psi}(\omega), \quad \text{Im } \tau \leq 0. \quad (\text{A1})$$

It follows that $\psi^+(\tau)$ is an analytic function in the lower half of the complex τ plane. This function may also be defined directly from the *real* data $\psi(t)$ for real t via

$$\psi^+(\tau) = \frac{1}{\pi i} \int_{-\infty}^\infty dt \frac{\psi(t)}{\tau - t}, \quad \text{Im } \tau \leq 0. \quad (\text{A2})$$

From (A2), the limit of ψ on the real t axis is related to the real signal $\psi(\tau)$ via

$$\psi^+(t) = \psi(t) + i\bar{\psi}(t), \quad t \text{ real}, \quad (\text{A3})$$

where

$$\bar{\psi}(t) = \frac{-1}{\pi} \int_{-\infty}^\infty dt' \mathcal{P} \frac{\psi(t')}{t - t'}$$

is the Hilbert transform, with \mathcal{P} denoting Cauchy's principal value. The real signal for real t can therefore be recovered via $\psi(t) = \text{Re } \psi^+(t)$.

Thus, if $p(\mathbf{r}, t)$ is an analytic solution of the time-dependent wave equation, then both $p_r = \text{Re } p$ and $p_i = \text{Im } p$ are real solutions of the wave equation. Henceforth, we shall only consider p_r since p_i or any other linear combination of p_r and p_i can be obtained by multiplying p by a complex constant and then taking the real part.

APPENDIX B: ADDITIONAL PROPERTIES OF THE OS SYSTEM

From (2.8), one may readily infer the following relations:

$$s_r^2 - s_i^2 = r^2 - b^2, \quad s_r s_i = -zb, \quad (\text{B1})$$

$$\nabla s_r = (\mathbf{r} s_r - \mathbf{b} s_i) / |s|^2, \quad |\nabla s_r| = \sqrt{b^2 + s_r^2} / |s|, \quad (\text{B2})$$

$$\nabla s_i = -(\mathbf{r} s_i + \mathbf{b} s_r) / |s|^2, \quad |\nabla s_i| = \sqrt{b^2 - s_i^2} / |s|, \quad (\text{B3})$$

$$\nabla s_r \cdot \nabla s_i = 0, \quad (\text{B4})$$

and the metric coefficients⁴⁰ along the (s_r, s_i, ϕ) coordinates are

$$h_{s_r} = |s| / \sqrt{b^2 + s_r^2}, \quad h_{s_i} = |s| / \sqrt{b^2 - s_i^2}, \quad (\text{B5})$$

$$h_\phi = b^{-1} \sqrt{b^2 + s_r^2} \sqrt{b^2 - s_i^2}.$$

¹E. Heyman and B. Z. Steinberg, "A spectral analysis of complex source pulsed beams," J. Opt. Soc. Am. **A 4**, 473–480 (1987).

²E. Heyman and L. B. Felsen, "Complex source pulsed beam fields," J. Opt. Soc. Am. **A 6**, 806–817 (1989).

³E. Heyman, B. Z. Steinberg, and R. Ianculescu, "Electromagnetic complex source pulsed beam fields," IEEE Trans. Antennas Propag. **AP-38**, 957–963 (1990).

⁴G. A. Deschamps, "Gaussian beams as a bundle of complex rays," Electron. Lett. **7**, 684–685 (1971).

- ⁵J. W. Ra, H. Bertoni, and L. B. Felsen, "Reflection and transmission of beams at dielectric interfaces," *SIAM (Soc. Ind. Appl. Math.) J. Appl. Math.* **24**, 396–412 (1973).
- ⁶L. B. Felsen, "Complex-source-point solutions of the field equations and their relation to the propagation and scattering of Gaussian beams," in *Symposia Matematica, Istituto Nazionale di Alta Matematica* (Academic, London, 1976), Vol. XVIII, pp. 40–56.
- ⁷S. Y. Shin and L. B. Felsen, "Gaussian beam modes by multipoles with complex source points," *J. Opt. Soc. Am.* **67**, 699–700 (1977).
- ⁸G. Kaiser, *A Friendly Guide to Wavelets* (Birkhauser, Boston, 1994), pp. 276–279.
- ⁹E. Heyman, R. Strachievitz, and D. Koslof, "Pulsed beam reflection and transmission at a planar interface: Exact solutions and approximate local models," *Wave Motion* **18**, 315–343 (1993).
- ¹⁰R. Ianculescu and E. Heyman, "Pulsed beam diffraction by a perfectly conducting wedge. I. Exact solution," *IEEE Trans. Antennas Propag.* **AP-42**, 1377–1385 (1994).
- ¹¹E. Heyman and R. Ianculescu, "Pulsed beam diffraction by a perfectly conducting wedge. Part II: Local scattering models," *IEEE Trans. Antennas Propag.* **AP-43**, 519–528 (1995).
- ¹²E. Heyman, "Pulsed beam propagation in an inhomogeneous medium," *IEEE Trans. Antennas Propag.* **AP-42**, 311–319 (1994).
- ¹³A. N. Norris, B. S. White, and J. R. Schrieffer, "Gaussian wave packets in inhomogeneous media with curved interfaces," *Proc. R. Soc. London, Ser. A* **412**, 93–123 (1987).
- ¹⁴E. Heyman, A. G. Tijhuis, and J. Boersma, "Spherical and collimated pulsed fields in conducting media," *Proceedings of URSI Trium International Symposium on Electromagnetic Theory, St. Petersburg, 1995*, pp. 643–645 (unpublished).
- ¹⁵T. Melamed and L. B. Felsen, "Pulsed beam propagation in lossless dispersive media. I. Theory," *J. Opt. Soc. Am. A* **15**, 1268–1276 (1998).
- ¹⁶T. Melamed and L. B. Felsen, "Pulsed beam propagation in lossless dispersive media. Part II. Applications," *J. Opt. Soc. Am. A* **15**, 1277–1284 (1998).
- ¹⁷J. Oz and E. Heyman, "Modal theory for the two-frequency mutual coherence function in random media. Beam waves," *Waves Random Media* **8**, 159–174 (1998).
- ¹⁸J. Gozani, "Pulsed beam propagation through random media," *Opt. Lett.* **21**, 1712–1714 (1996).
- ¹⁹S. Zeroug, F. E. Stanke, and R. Burrige, "A complex-transducer-point model for finite emitting and receiving ultrasonic transducers" *Wave Motion* **24**, 21–40 (1996).
- ²⁰S. Feng and H. G. Winful, "Spatiotemporal transformations of isodiffracting ultrashort pulses by nondispersive quadratic phase media," *J. Opt. Soc. Am. A* **16**, 2500–2509 (1999).
- ²¹M. A. Porras, "Ultrashort pulsed Gaussian light beams," *Phys. Rev. E* **58**, 1086–1093 (1998).
- ²²M. A. Porras, "Nonsinusoidal few-cycle pulsed light beams in free space," *J. Opt. Soc. Am. B* **16**, 1468–1474 (1999).
- ²³E. Heyman, "Complex source pulsed beam expansion of transient radiation," *Wave Motion* **11**, 337–349 (1989).
- ²⁴B. Z. Steinberg, E. Heyman, and L. B. Felsen, "Phase space beam summation for time dependent radiation from large apertures: Continuous parametrization," *J. Opt. Soc. Am. A* **8**, 943–958 (1991).
- ²⁵B. Z. Steinberg and E. Heyman, "Phase space beam summation for time dependent radiation from large apertures: Discretized parametrization," *J. Opt. Soc. Am. A* **8**, 959–966 (1991).
- ²⁶T. Melamed, "Phase space beam summation: A local spectrum analysis of time dependent radiation," *J. Electromagn. Waves Appl.* **11**, 739–773 (1997).
- ²⁷E. Heyman and I. Beracha, "Complex multipole pulsed beams and Hermite pulsed beams: A novel expansion scheme for transient radiation from well collimated apertures," *J. Opt. Soc. Am. A* **9**, 1779–1793 (1992).
- ²⁸T. B. Hansen and A. N. Norris, "Exact complex source representations of transient radiation," *Wave Motion* **26**, 101–115 (1997).
- ²⁹T. Melamed, E. Heyman, and L. B. Felsen, "Local spectral analysis of short-pulse-excited scattering from weakly inhomogeneous media. I. Forward scattering," *IEEE Trans. Antennas Propag.* **AP-47**, 1208–1217 (1999).
- ³⁰T. Melamed, E. Heyman, and L. B. Felsen, "Local spectral analysis of short-pulse-excited scattering from weakly inhomogeneous media. II. Inverse scattering," *IEEE Trans. Antennas Propag.* **AP-47**, 1218–1227 (1999).
- ³¹J. N. Brittingham, "Focus wave modes in homogeneous Maxwell's equations: Transverse electric mode," *J. Appl. Phys.* **54**, 1179–1189 (1983).
- ³²R. W. Ziolkowski, "Exact solutions of the wave equation with complex source locations," *J. Math. Phys.* **26**, 861–863 (1985).
- ³³A. M. Shaarawi, I. M. Besieris, R. W. Ziolkowski, and S. M. Sedky, "The generation of approximate focus wave mode pulses from wide-band dynamic Gaussian apertures," *J. Opt. Soc. Am. A* **12**, 1954–1964 (1995).
- ³⁴E. Heyman, "The focus wave mode: A dilemma with causality," *IEEE Trans. Antennas Propag.* **AP-37**, 1604–1608 (1989).
- ³⁵J. Durnin, J. J. Miceli, Jr., and J. H. Eberly, "Diffraction free beam" *Phys. Rev. Lett.* **58**, 1499–1452 (1987).
- ³⁶J.-y. Lu and J. F. Greenleaf, "Nondiffracting X waves—exact solutions to free space scalar wave equation and their finite aperture realizations," *IEEE Trans. Ultrason. Ferroelectr. Freq. Control* **39**, 19–31 (1992).
- ³⁷H. E. Moses and R. T. Prosser, "Initial conditions, sources, and currents for prescribed time-dependent acoustic and electromagnetic fields in three dimensions. I. The inverse initial value problem. Acoustic and electromagnetic "bullets," expanding waves, and imploding waves," *IEEE Trans. Antennas Propag.* **AP-34**, 188–196 (1986).
- ³⁸H. E. Moses and R. T. Prosser, "Acoustic and electromagnetic bullets. New exact solutions of the acoustic and Maxwell's equation," *SIAM (Soc. Ind. Appl. Math.) J. Appl. Math.* **50**, 1325–1340 (1990).
- ³⁹A. Shlivinski and E. Heyman, "Time domain near field analysis of short pulse antennas. Part I: Spherical wave (multipole) expansion;" "Part II Reactive energy and the antenna Q ," *IEEE Trans. Antennas Propag.* **AP-47**, 271–279 (1999); **AP-47**, 280–286 (1999).
- ⁴⁰J. A. Stratton, *Electromagnetic Theory* (McGraw-Hill, New York, 1941).